

Magnetic and electronic properties of a single crystal of ordered double perovskite $\text{Sr}_2\text{FeMoO}_6$

Y. Tomioka, T. Okuda, Y. Okimoto, R. Kumai, and K.-I. Kobayashi

Joint Research Center for Atom Technology (JRCAT), 1-1-4 Higashi, Tsukuba 305-0046, Japan

Y. Tokura

Joint Research Center for Atom Technology (JRCAT), 1-1-4 Higashi, Tsukuba 305-0046, Japan

and Department of Applied Physics, University of Tokyo, 7-3-1 Hongo, Tokyo 113-8656, Japan

(Received 16 July 1999)

A single crystal of ordered double perovskite oxide $\text{Sr}_2\text{FeMoO}_6$, a conducting ferromagnet with $T_C \sim 420$ K, has been prepared by the floating zone method, and the magnetic and electronic properties have been investigated. It has been found that the ordinary and anomalous Hall coefficients are negative and positive, respectively, and that the density of the conduction electrons is estimated at $1.1 \times 10^{22} \text{ cm}^{-3}$, corresponding to nearly one electron-type carrier per a pair of Fe and Mo. The electronic specific heat is about $8 \text{ mJ}/(\text{mol K}^2)$ in accord with the result of the band-structure calculation by the local density functional (LDA) method. In the optical conductivity spectrum, interband transitions from Fe e_g to Mo t_{2g} band with up spin across the Fermi level and from the O 2_p to the Mo/Fe t_{2g} band with down spin are observed at 0.5 eV and 3.9 eV, respectively, which confirms the half-metallic electronic structure predicted by the LDA calculation.

I. INTRODUCTION

In the complex oxides with the ordered perovskite structure, $A_2B'B''O_6$ (A being alkaline-earth or rare-earth elements, while B' and B'' being different transition-metal ones, respectively),¹ the B' and B'' cations are alternately ordered in a rock-salt lattice, as schematically shown in Fig. 1, partly due to a large difference in their charges or ionic radii.¹ For instance, a lattice of $A_2\text{FeMoO}_6$ ($A = \text{Ba}, \text{Sr}, \text{and Ca}$) shows an alternate ordering of Fe^{3+} and Mo^{5+} at the B' and B'' sites, respectively. In $\text{Sr}_2\text{FeMoO}_6$, the crystal symmetry is known as cubic² or tetragonal³ with the regular arrangement of the alternating FeO_6 and MoO_6 octahedra. In the localized-spin model, the magnetic interaction between Fe and Mo having the Fe-O-Mo angle of $\approx 180^\circ$ appears antiferromagnetic,³ and hence may produce a ferrimagnetic ground state, although the actual compound is metallic and the localized-spin picture is too naive. The observed magnetic (ferromagnetic or ferrimagnetic) transition temperature for $\text{Sr}_2\text{FeMoO}_6$ is as high as 410–450 K (Refs. 1–4).

A renewed interest in these ordered perovskites has recently been aroused in connection with gigantic magnetoresistance,⁵ that has typically been observed for perovskite and layered-perovskite manganites. At the ferromagnetic ground state of manganites (e.g., $\text{La}_{1-x}\text{Sr}_x\text{MnO}_3$ with $x \sim 0.3$), a density of states near the Fermi level is composed only of up-spin electrons, giving rise to a half-metallic nature. In this case, an energy gap between the up-spin and the down-spin conduction band is due to a strong Hund's-rule coupling between the local t_{2g} and itinerant e_g electrons. Such a close interplay between the magnetic and electronic states as observed for manganites is expected also for the ordered perovskites. For $\text{Sr}_2\text{FeMoO}_6$, a density-functional calculation of the electronic structure has recently been carried out with the generalized gradient approximation (GGA) by Sawada and Terakura.^{5,6} The results show that the occupied up-spin band mainly comes from the Fe $3d$ electrons.

The Fermi level exists within the down-spin band, which is composed of Fe t_{2g} and Mo t_{2g} electrons. As an intuitive picture for the electronic state, the electrons of Fe and Mo cations may be considered as localized and itinerant, respectively, with the valence states of Fe^{3+} ($3d^5$; $t_{2g}^3 e_g^2$, $S = \frac{5}{2}$) and Mo^{5+} ($4d^1$; t_{2g}^1 , $S = \frac{1}{2}$). Taking the magnetic interaction (interatomic antiferromagnetic exchange) between Fe and Mo into account, a ferrimagnetic half-metallic state⁷ is expected for this ordered perovskite with localized up-spins of Fe^{3+} and itinerant down-spin electron of Mo^{5+} . The s - d (or Kondo lattice) model may be applicable to the unique magnetic and electronic properties of ordered perovskites as such a conducting ferrimagnet.

A high spin-polarization of conduction carriers expected for $\text{Sr}_2\text{FeMoO}_6$ is attractive also in the light of the potential application to the magnetoresistive devices. A late investigation on the polycrystalline specimen of $\text{Sr}_2\text{FeMoO}_6$ (Ref. 5) has reported a fairly-large magnetoresistance (MR) subsisting up to room temperature, that has been interpreted in terms of the intergrain tunneling of spin-polarized electrons. A relatively high magnetic transition temperature (410–450

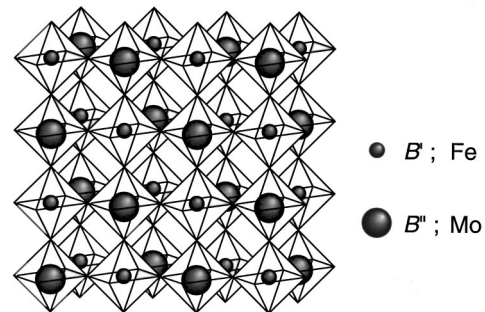


FIG. 1. A schematic picture of alternating $B'O_6$ and $B''O_6$ octahedra in an ordered perovskite structure $A_2B'B''O_6$. In $\text{Sr}_2\text{FeMoO}_6$, the Fe and Mo cations occupy the B' and B'' sites, respectively.

TABLE I. Structural data determined from a single crystal x-ray diffraction.

Formula weight	Crystal system	Space group	Lattice parameters (Å)	V (Å ³)	d_{cal} (g/cm ³)
423.02	Tetragonal	$14/mmm$	$a_0=5.577(3)$, $a_0=7.887(4)$	245.3(1)	5.73

K) indicates that a spin-polarization of conduction electrons remains relatively high (70%) even at room temperature, provided that the ground state is a half metal.

At this stage, a study with use of a high-quality single crystal is desired to further investigate the issues described hitherto. In this paper, we report magnetic and electronic properties relevant to the half-metallic state of the $\text{Sr}_2\text{FeMoO}_6$ single crystal prepared by the floating-zone method. Following the description of the experimental procedures (Sec. II), the floating-zone synthesis and structural characterization of a single crystal are by first described (Sec. III A). Subsequently, the transport properties (Sec. III B), electronic and magnetic specific heat (Sec. III C) are presented. The electronic structure is investigated by optical spectroscopy (Sec. III D), and comparison with the calculated band structure is made. The summary is given in Sec. IV.

II. EXPERIMENTAL PROCEDURES

The samples of $\text{Sr}_2\text{FeMoO}_6$ used in various measurements were single crystals, which were grown by the floating-zone method as described in detail in Sec. III A. Magnetization data up to 5 T have been taken by a commercial superconducting quantum interference device magnetometer. The resistivity and Hall effect have been measured in magnetic fields up to 7 T using a cryostat equipped with a superconducting magnet. For the Hall effect measurement, a piece of crystal was formed into a rectangular shape with typical dimensions of 5 (length) \times 1.3 (width) \times 0.13 (thickness) mm³, and the gold wires were attached to a rectangular sample through the electrodes made by gold paste. To remove the asymmetric voltage, three terminals (one at one edge and two in the other edge) were attached and the offset voltage was canceled by adjusting the variable resistance connecting to the two terminals.

For the specific-heat measurement in magnetic fields (up to 9 T), the sample is mounted on a sapphire chip, and the data ($0.5 < T < 10$ K) have been collected by the relaxation method. We measured reflectivity spectra [$R(\omega)$] for a crystal of $\text{Sr}_2\text{FeMoO}_6$ with a typical size of ~ 5 mm ϕ (ϕ : diameter). $R(\omega)$ in the infrared range 0.06–0.8 eV were measured using a Fourier transform type interferometer with a MCT detector. A grating type monochromator was used for the higher-energy range, 0.6–36 eV. For the measurement above 5 eV, we made use of synchrotron radiation at UV-SOR, Institute for Molecular Science. In order to investigate the optical spectra at low-temperature 10 K, we measured $R(\omega)$ using He-cryostat up to 5.0 eV. As a reference mirror, we used evaporated Ag film on the crystal (0.06–2.9 eV), and Al film (above 2.8–5 eV). Namely, the spectrum at 10 K was measured from 0.06 to 5 eV and extrapolated by the data above 4.9 eV at room temperature. The optical conductivity spectra were obtained by Kramers-Kronig analysis of $R(\omega)$. For this analysis, we assumed Hagen-Rubens type extrapo-

lation below 0.06 eV. For the higher-energy reflectivity above 36 eV, the ω^{-4} -type extrapolation was used.

III. RESULTS AND DISCUSSION

A. Synthesis and characterization of a $\text{Sr}_2\text{FeMoO}_6$ single crystal

The polycrystalline sample was first synthesized by sintering a stoichiometric mixture of SrCO_3 , Fe_2O_3 , and MoO_3 at 1270 °C for 12 h in a flow of $\text{H}_2(7\%)/\text{Ar}$. A result of x-ray diffraction indicated that the powder was in a single phase. (The reactions in air were not successful for the formation of ordered perovskite structure, but resulted in formation of subphases, such as SrMoO_4 .) The obtained powder was pulverized and formed into a rod with about 100 mm in length and 5 mm in diameter. A rod was sintered for 12–24 h under the same condition as used in synthesis of the polycrystalline sample.

The crystal growth was performed in a floating-zone furnace equipped with double hemiellipsoidal mirrors coated with gold. Two halogen lamps were used as heat sources. A single crystal was grown in argon atmosphere at a growth rate of 15–20 mm/h with rotating seed and feed rods in opposite directions. The formation of a single crystal was confirmed by a Laue reflection method and it was found that a growth direction is parallel to $[111]_c$ direction of the pseudocubic setting. Then, a part of a melt-grown rod was pulverized and characterized by an x-ray diffraction, which confirmed that the melt-grown sample is a single phase of the ordered perovskite structure. The powder diffraction pattern was consistent with the tetragonal $14/mmm$ symmetry, and a Rietveld refinement gave that $a_0=5.571(2)$ Å and $c_0=7.889(4)$ Å. A degree of Fe/Mo ordering of the melt-grown crystal was estimated to be about 85% from an intensity of the superstructure reflections from $(h k l)$ with l odd, e.g., $(1 0 1)$. The cation ratio of the melt-grown crystal was also checked by an inductively coupled plasma spectroscopy, and the ratios of Sr/(Fe+Mo) and Fe/Mo were determined as 1.01 and 0.988, respectively. To improve the ordering of Fe and Mo, the as-grown crystal was annealed at 1250 °C for 12 h in a flow of $\text{H}_2(4\%)/\text{Ar}$, and it was cooled to room temperature at a speed of 50 °C/h. A part of the annealed crystal was pulverized and characterized by a powder x-ray diffraction, which indicated that the Fe/Mo ordering was increased from 85% to 92%. The following of this paper is describing a study on the annealed crystal.

To further investigate the crystal structure, a single crystal x-ray diffraction was performed with use of a four-circle diffractometer with graphite-monochromated Mo $K\alpha$ radiation. The diffraction data were automatically collected with use of MSC/AFC diffractometer software of the Molecular Structure Corporation, and the total numbers of reflections by the ω - 2θ method were 368. The structural parameters of a $\text{Sr}_2\text{FeMoO}_6$ crystal are listed in Table I. Subsequently, the

TABLE II. The refined atomic parameters at room temperature for an annealed crystal of $\text{Sr}_2\text{FeMoO}_6$ with 92% ordering of Fe and Mo ($R=0.037$, $R_{\text{wp}}=0.041$).

Atom	Positions	x	y	z	g^a	$B_{\text{eq}} (\text{\AA}^2)^b$	$U_{11},^c U_{22}, U_{33} (\text{\AA}^2)$
Sr	$4d$	$\frac{1}{2}$	0	$\frac{1}{4}$	1	0.55(3)	0.0075(9), 0.0075(9), 0.006(1)
Fe (1)	$2a$	0	0	0	0.92	0.38(10)	0.005(4), 0.005(4), 0.004(3)
Mo (1)	$2a$	0	0	0	0.08	0.0943	0.0017, 0.0017, 0.0002
Fe (2)	$2b$	0	0	$\frac{1}{2}$	0.08	0.38(10)	0.005(4), 0.005(4), 0.004(3)
Mo (2)	$2b$	0	0	$\frac{1}{2}$	0.92	0.0943	0.0017, 0.0017, 0.0002
O (1)	$8h$	0.249(3)	0.249(3)	$\frac{1}{2}$	1	1.3(2)	0.013(4), 0.013(4), 0.024(8)
O (2)	$4e$	0	0	0.254(4)	1	1.6(2)	0.029(9), 0.029(9), 0.0000

^aThe populations for Fe and Mo atoms were fixed at the values of 92% ordering (not refined).

^bThe thermal factor is represented as the equivalent isotropic displacement parameter (B_{eq}).

^cThe anisotropic displacement parameters (U_{11} , U_{22} , and U_{33}) are estimated with use of the relation that $B_{\text{eq}} = (8\pi^2/3) [U_{11}(ad^*)^2 + U_{22}(bb^*)^2 + U_{33}(cc^*)^2 + 2U_{12}aa^*bb^* \cos \gamma + 2U_{23}bb^*cc^* \cos \alpha + 2U_{13}cc^*aa^* \cos \beta]$.

data were analyzed with use of the *teXsan* crystallographic software package of the Molecular Structure Corporation. The atomic parameters were refined for an annealed crystal of $\text{Sr}_2\text{FeMoO}_6$ with Fe/Mo ordering of 92%, which confirmed the tetragonal $I4/mmm$ symmetry consistent with the results of the powder x-ray diffraction ($R=0.037$, $R_{\text{wp}}=0.041$). The atomic parameters refined are listed in Table II. As shown in Table II, the atomic positions for O(1) and O(2) indicate slight displacements toward Mo atom. In $\text{Sr}_2\text{FeMoO}_6$, therefore, the size of MoO_6 octahedra seems to be smaller than that of FeO_6 octahedra.

B. Transport properties

Figure 2 shows the temperature profiles of (a) magnetization and (b) resistivity in magnetic fields of a $\text{Sr}_2\text{FeMoO}_6$ single crystal. In Fig. 2(a), the magnetization at 0.5 T per a formula unit of $\text{Sr}_2\text{FeMoO}_6$ is $\sim 2.9 \mu_B$ (and increases up to a saturated value of $\sim 3.2 \mu_B$ at high fields as shown in the inset) at the lowest temperature and it is still appreciable at 400 K. The resistivity measurement up to 500 K has indicated some anomaly around 420 K, which perhaps corresponds to the Curie temperature (T_C). The T_C value is in good agreement with that in literature (Refs. 1 and 2). In Fig. 2(b), the resistivity (ρ) shows a metallic behavior ($d\rho/dT > 0$) down to the lowest temperature, and no significant MR effect is seen apart from small MR at temperatures below about 150 K. The small negative MR is perhaps due to the antisite defects at the Fe and Mo sites as argued below. These features shown in Fig. 2(b) are quite in contrast to those of the polycrystalline specimen, which shows a large negative MR ($\Delta\rho/\rho \approx 0.3$ at 7 T) (Ref. 5). In other words, the absence of appreciable MR in the single crystal as observed in Fig. 2(b) confirms the assignment made in Ref. 5 that a fairly large MR of a polycrystalline specimen of $\text{Sr}_2\text{FeMoO}_6$ is due to field-induced change in carrier scattering at the grain boundaries that are characteristic of ceramics.^{8,9}

The relatively low saturation moment ($\approx 3.2 \mu_B$), as compared with the ideal value ($4 \mu_B$; $S_{\text{total}} = \frac{5}{2} - \frac{1}{2} = 2$) is accounted for in terms of the antisite defects at the B_{Fe} and B_{Mo} sites.^{5,6} If a Mo^{5+} ($S = \frac{1}{2}$) is at the B_{Fe} site surrounded by the Mo^{5+} neighbors, its magnetic moment tends to be parallel to those of the Mo^{5+} ions, which decreases the net magnetiza-

tion by $6 \mu_B$. Inversely, if a Fe^{3+} ($S = \frac{5}{2}$) is at a B_{Mo} site, its magnetic moment tends to be antiparallel to those of the Fe^{3+} ions, causing a decrease in the net magnetization by $4 \mu_B$. Hence, the total decrease in magnetization per a pair of the antisite defects is as large as $10 \mu_B$. This estimate of the magnetization loss indicates that the observed decrease by

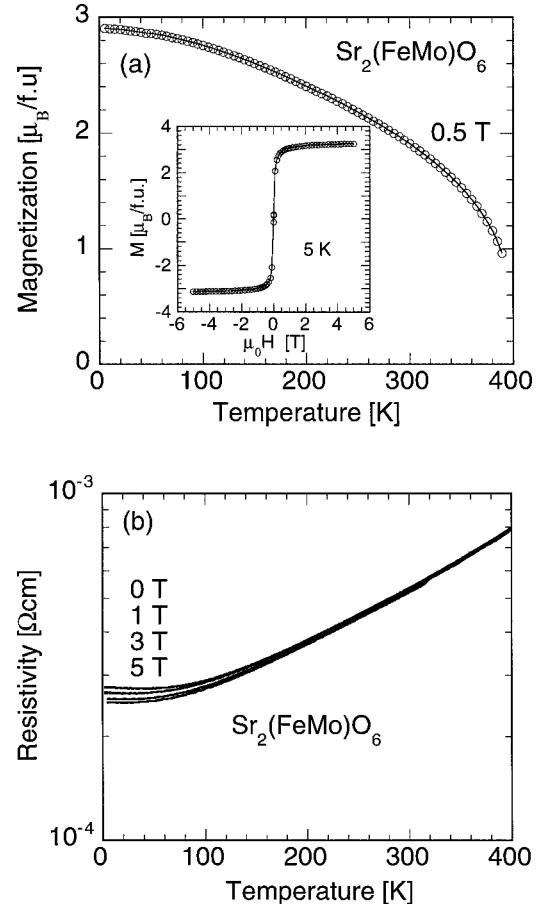


FIG. 2. (a) The temperature profiles of magnetization for a single crystal of $\text{Sr}_2\text{FeMoO}_6$ taken at 0.5 T. The inset shows a magnetization hysteresis curve for the same crystal taken at 5 K. (b) Temperature profiles of resistivity in several magnetic fields for a $\text{Sr}_2\text{FeMoO}_6$ crystal.

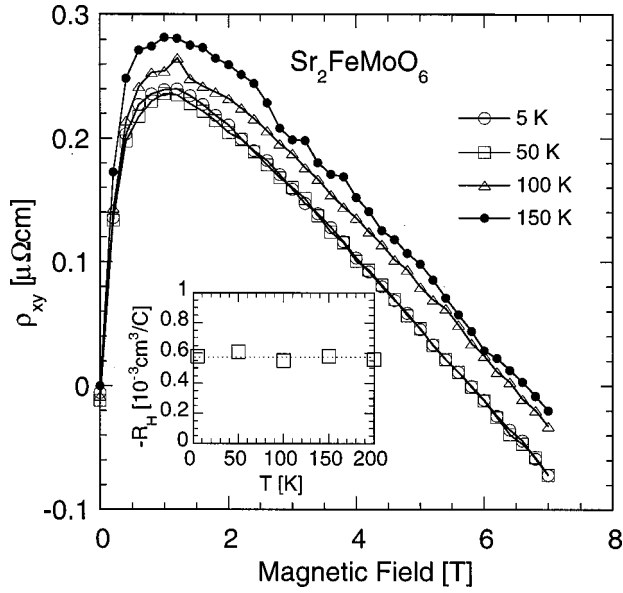


FIG. 3. The magnetic field dependence of the Hall resistivity ρ_{xy} taken at several temperatures for a single crystal of $\text{Sr}_2\text{FeMoO}_6$. Inset shows the temperature dependence of the inversed ordinary Hall coefficient ($1/R_H$). The ordinary Hall coefficient is obtained from the slope $d\rho_{xy}/dH$ at $\mu_0 H > 1$ T. The dotted line is the guide to the eyes.

$0.8\mu_B$ from the ideal value is expected if the antisite defects exist in a portion of 8% at the Fe and Mo sites, which is consistent with the result of powder x-ray diffraction.

Figure 3 shows the magnetic field dependence of Hall resistivity ρ_{xy} of a $\text{Sr}_2\text{FeMoO}_6$ crystal taken at several temperatures. The ρ_{xy} first increases at $0 < \mu_0 H < 1$ T, which is ascribed to an anomalous Hall effect, and then turn decreases at $\mu_0 H > 1$ T. The slope $d\rho_{xy}/dH$ at $\mu_0 H \geq 1$ T is negative and almost temperature independent. In magnetic substances, both of the ordinary and anomalous parts contribute to the Hall effect. Taking a demagnetizing effect into account, the Hall resistivity ρ_{xy} is represented as¹⁰

$$\rho_{xy} = R_H + R_1 M, \quad (1)$$

where $R_1 = (1 - N)R_H + R_S$. Here, R_H and R_S are the ordinary and anomalous Hall coefficient, respectively. The H , M , and N are an external magnetic field, magnetization, and a demagnetizing factor of a sample, respectively. Since the magnetization of a $\text{Sr}_2\text{FeMoO}_6$ crystal almost reaches saturation for $\mu_0 H > 1$ T, the ordinary Hall coefficient is determined from the value of $d\rho_{xy}/dH$ in a high-field region. The inset to Fig. 3 shows the temperature dependence of the obtained R_H . The R_H has a negative sign, that is, the conduction carrier is electronlike. With use of the relation that $R_H = 1/(en)$, a density of conduction carriers is estimated to be $\approx 1.1 \times 10^{22} \text{ cm}^{-3}$ (approximately one electron per a pair of Fe and Mo), which shows no significant dependence on temperature below 200 K. These results obtained by the ordinary Hall effect seem to be consistent with the density-functional calculation based on generalized gradient approximation (GGA) (Ref. 5) that indicates a metallic Fermi surface.

As indicated in Eq. (1), the anomalous Hall coefficient can be obtained through $R_1 M$. In Fig. 3, the value of $R_1 M_S$ (M_S being the saturation moment) is obtained as an intercept

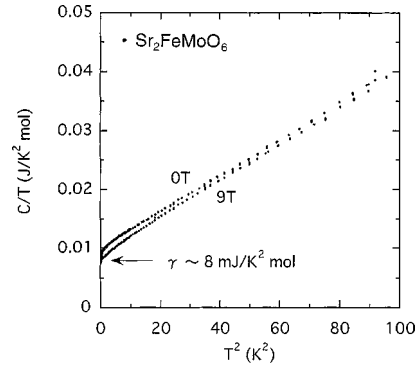


FIG. 4. The specific heat, C/T vs T^2 , for a $\text{Sr}_2\text{FeMoO}_6$ crystal taken at zero magnetic field and 9 T. The electronic specific heat coefficient γ is given as an intercept of the C/T vs T^2 line at 9 T on the ordinate.

of the $\rho_{xy} - H$ line at $\mu_0 H > 1$ T on the ordinate. The anomalous Hall coefficient is then evaluated with use of the relation that $R_1 = (1 - N)R_H + R_S$. At 5 K, for instance, R_S is estimated at $1.16 \times 10^{-10} \text{ } \Omega \text{ cm/G}$ with $R_1 M = 0.335 \text{ } \mu\Omega \text{ cm}$, $M = 2802 \text{ G}$, $N \sim 0.9$ (Ref. 11) and $R_H = -0.578 \times 10^{-3} \text{ cm}^3/\text{C}$. It is noted in Fig. 3 that the sign of R_S is positive opposite to that of R_H . This is in contrast to the case of conventional ferromagnets, Fe and Ni, the both R_H and R_S of which have the same sign. Perovskite manganites, say $\text{La}_{1-x}\text{Sr}_x\text{MnO}_3$, as another typical half-metal shows the positive R_H and negative R_S oppositely to the present case. The R_S for the manganites becomes vanishingly small as the temperature (or spin fluctuation) tends to zero. By contrast, the R_S of $\text{Sr}_2\text{FeMoO}_6$ is rather temperature-independent in spite of apparently half-metallic character. An origin of such an unconventional behavior of the R_S is left to be elucidated, but might be relevant to some magnetic frustration arising from the mis-site imperfections.

C. Electronic and magnetic specific heat

To further quantify the electronic properties of $\text{Sr}_2\text{FeMoO}_6$, the low-temperature specific heat has been measured. In the case of magnetically ordered states, the contribution from the spin-wave excitation is additional to the specific heat. Then, the total specific heat is composed of three parts; namely, contributions from conduction electron, spin waves, and lattice, represented as

$$C = C_{\text{el.}}(T) + C_{\text{SW}}(T) + C_{\text{lattice}}(T) = \gamma T + \alpha T^{3/2} + \beta T^3. \quad (2)$$

Here, γ is the electronic specific heat coefficient, while α and β are related with the spin wave excitation and the Debye temperature, respectively.

Figure 4 shows the C/T vs T^2 of a $\text{Sr}_2\text{FeMoO}_6$ crystal, which was taken at zero magnetic field and 9 T. Below about 10 K, application of an external magnetic field of 9 T is sufficient to cause a spin-wave gap and remove a spin-wave contribution from a specific heat. Therefore, an intercept of the $C/T - T^2$ line at 9 T on the ordinate gives that $\gamma \sim 8 \text{ mJ}/(\text{mol K}^2)$, as shown in Fig. 4. In a conventional metal, the electronic specific heat is related to the density of states at the Fermi level $N(E_F)$ via the relation that γ

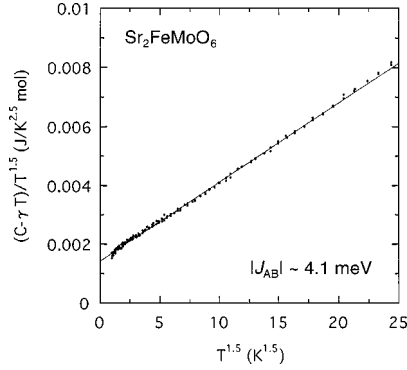


FIG. 5. The specific heat from which the electronic part is subtracted, $(C - \gamma T)/T^{3/2}$ vs $T^{3/2}$, for a $\text{Sr}_2\text{FeMoO}_6$ crystal.

$= 1/3 \pi^2 k_B^2 N(E_F)$. In the present case, $N(E_F)$ is calculated as $2.0 \times 10^{24} \text{ eV}^{-1} \text{ mol}^{-1}$, which is consistent with the LDA result ($1.2 \times 10^{24} \text{ eV}^{-1} \text{ mol}^{-1}$) (Ref. 5) but may be somewhat renormalized by the electron-correlation effect. Incidentally, the temperature (T) dependence of the resistivity is quadratic with T in this crystal, and a coefficient A in $\rho(T) = \rho_0 + AT^2$ is about $2.16 \times 10^{-3} \mu\Omega \text{ cm/K}^2$. This gives the ratio $A/\gamma^2 \approx 3.3 \times 10^{-5} \mu\Omega \text{ cm}/(\text{mJ K}^{-1} \text{ mol}^{-1})^2$, being not contradictory to the Kadowaki-Wood law that $A/\gamma^2 = 1.0 \times 10^{-5} \mu\Omega \text{ cm}/(\text{mJ K}^{-1} \text{ mol}^{-1})^2$ (Ref. 12).

By utilizing the value of γ , the electronic part can be subtracted from the net specific heat, which makes it possible to estimate the value of α in Eq. (2). Figure 5 shows the $(C - \gamma T)/T^{3/2}$ vs $T^{3/2}$. The $(C - \gamma T)/T^{3/2}$ is almost linearly dependent on $T^{3/2}$ at such low temperatures. An intercept of the $(C - \gamma T)/T^{3/2}$ vs $T^{3/2}$ line on the ordinate gives that $\alpha = 1.45 \text{ mJ}/(\text{K}^{2.5} \text{ mol})$.

A contribution from spin waves $C_{\text{sw}}(T)$ ($= \alpha T^{3/2}$) in Eq. (2) is further written as (N_0 and k_B being the Avogadro number and the Boltzmann constant, respectively)

$$C_{\text{sw}}(T) (= \alpha T^{3/2}) = 0.113 N_0 k_B A^{3/2} (k_B T)^{3/2}, \quad (3)$$

where $A = (S_A - S_B)/(4J_{AB}S_A S_B)$ in the case of a ferrimagnet with S_i and J_{ij} being the spin quantum number at i sublattice and the exchange interaction between i and j sublattices, respectively.¹³ With the values of $\alpha = 1.45 \text{ mJ}/(\text{K}^{2.5} \text{ mol})$, $S_A = \frac{5}{2}$, and $S_B = \frac{1}{2}$, one obtains $J_{AB} = -4.1 \text{ meV}$. According to a mean-field theory on the ferrimagnet, the simplest approximation gives the Curie temperature as $T_C = w(C_A C_B)^{1/2}$, where $w = -2zJ_{AB}/(N_0 g^2 \mu_B^2)$ (z , g , and μ_B being the coordination numbers, the Lande factor and the Bohr magneton, respectively) and $C_i = N_0 g^2 \mu_B^2 S_i(S_i + 1)/3k_B$. With $z = 6$ and $J_{AB} = -4.1 \text{ meV}$ for the present compound, the Curie temperature is thus evaluated to be $\approx 490 \text{ K}$, which shows a reasonable agreement with the observed value ($\approx 420 \text{ K}$).

D. Electronic structure investigated by optical spectroscopy

The issue discussed here is an electronic structure of $\text{Sr}_2\text{FeMoO}_6$ investigated by optical spectroscopy on a single-crystal specimen. Figure 6 shows (a) reflectivity spectrum and (b) converted optical conductivity spectrum $[\sigma(\omega)]$ in the ground state (10 K). For comparison, the electronic band structure of $\text{Sr}_2\text{FeMoO}_6$ as predicted by the band calculation⁵

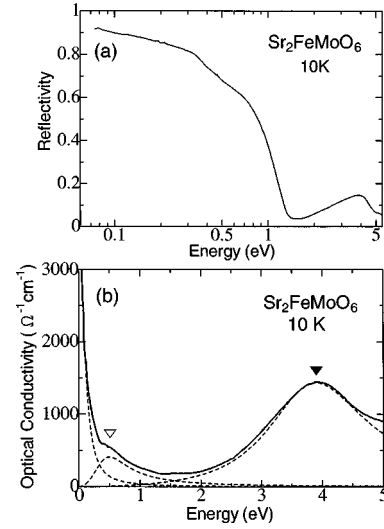


FIG. 6. The spectra of (a) optical reflectivity taken at 10 K and (b) converted optical conductivity for a $\text{Sr}_2\text{FeMoO}_6$ crystal. The d - d transition from Fe e_g to Mo t_{2g} band with up spin (at $\approx 0.5 \text{ eV}$) and the charge transfer (CT) transition from O $2p$ to Mo/Fe t_{2g} band with down spin (at $\approx 4 \text{ eV}$) are denoted by open and closed triangles in (b), respectively. Three broken lines in (b) represent Drude component, d - d transition and p - d CT transition, respectively, fit with the three-component Drude-Lorentz model function (see text).

is schematically shown in Fig. 7. In Fig. 6(a), a metallic high-reflectivity band appears with an apparent plasma edge at 1 eV. The $\sigma(\omega)$ in Fig. 6(b) represents a sharp Drude-like response, which shows a steep increase toward $\omega = 0$, confirming a metallic behavior in the ordered perovskite. In addition to the Drude-like component, we can see a small but clear structure denoted with an open triangle around 0.5 eV in Fig. 6(b). The LDA calculation of the density of states based on the GGA has revealed that the up-spin band shows a small gap between e_g and t_{2g} bands,⁵ as schematically shown in Fig. 7. Then, it is reasonable to ascribe this small absorption to the d - d ($e_g \rightarrow t_{2g}$) electron transition. (Note that such a d - d transition is not intra-atomic but corresponds to the charge transfer (CT) excitation from Fe to Mo site, and this is consistent with its small spectral weight.) Compared with the d - d absorption, an intense peak-structure is seen around 4 eV. This large absorption probably results from the CT excitation from O $2p$ to Mo/Fe t_{2g} band with down spin. In 3d transition-metal oxide perovskites, the energy of the CT excitation critically depends on the number of

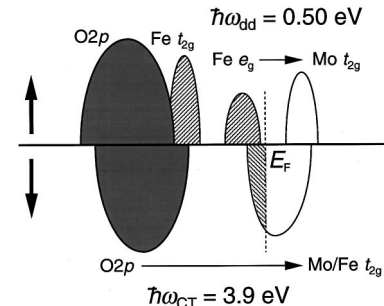


FIG. 7. A schematic picture of the electronic band structure of the ordered perovskite $\text{Sr}_2\text{FeMoO}_6$ based on the density-functional calculation by Sawada and Terakura (Ref. 5).

d -electrons.¹⁴ The single-peak structure of the present CT band indicates that Mo t_{2g} and Fe t_{2g} are so hybridized as to form an apparently single but broad final state in the optical process.

As shown by dotted lines in Fig. 6(b), the shape of $\sigma(\omega)$ can be divided into those three components, i.e., Drude component, d - d , and p - d CT transitions, and fit with a three-component curve by using conventional Drude-Lorentz model,

$$\begin{aligned}\sigma(\omega) &= \text{Im}[\omega\varepsilon(\omega)/4\pi] \\ &= \sigma(0)/\{1 + (\omega/\gamma_D)^2\} + (\omega/4\pi) \\ &\quad \times \text{Im}[S_{dd}\omega_{dd}^2/(\omega_{dd}^2 - \omega^2 + i\gamma_{dd}\omega) \\ &\quad + S_{CT}\omega_{CT}^2/(\omega_{CT}^2 - \omega^2 + i\gamma_{CT}\omega)].\end{aligned}\quad (4)$$

For fitting, we made use of the value of dc conductivity, $\sigma(0)$ (see Fig. 2). The estimated d - d and CT transition energies, $\hbar\omega_{dd}$ and $\hbar\omega_{CT}$, are 0.50 and 3.9 eV, respectively. In particular, a gap in the up-spin band across the Fermi level, which gives rise to a half-metallic nature for the down-spin band, is given by $\hbar\omega_{dd}$ (=0.50 eV). It is worth mentioning that those values of ω_{dd} and ω_{CT} show a quantitative agreement with the calculated band structure,⁵ again confirming the half-metallic nature of this compound as depicted in Fig. 7.

IV. SUMMARY

By utilizing single crystals prepared by the floating-zone method, we have investigated the electronic and magnetic properties of the ordered double perovskite oxide Sr₂FeMoO₆. The Curie temperature of a crystal is ~ 420 K and the saturation magnetization at the lowest temperature is

$\sim 3.2\mu_B$ per formula unit of Sr₂FeMoO₆. The deviation from the ideal value (= $4\mu_B$) may be ascribed to a significant reduction of the net moment due to $\sim 8\%$ of mis-site imperfections. The single crystal shows minimal MR effect, contrary to the case of polycrystalline samples, which shows prototypical intergrain tunneling MR. The ordinary and anomalous Hall coefficients are negative and positive, respectively, and the density of the conduction electrons is estimated to be $1.1 \times 10^{22} \text{ cm}^{-3}$, which corresponds to nearly one electron-type carrier per a pair of Fe and Mo. The electronic specific heat coefficient γ is about 8 mJ/(mol K²), or the density of states at E_F is $2.0 \times 10^{24} \text{ eV}^{-1} \text{ mol}^{-1}$, in overall agreement with the result of the electronic-structure calculation. From an analysis on the magnetic specific heat, we have estimated the ferrimagnetic interaction between Fe and Mo that $J_{AB} \approx -4.1$ meV, being consistent with the observed Curie temperature. In the optical conductivity spectrum, the lowest interband transition from Fe e_g to Mo t_{2g} band is observed at ≈ 0.5 eV, which corresponds to the gap value between the up-spin bands across the Fermi level. A charge-transfer transition from the $O2p$ to the Mo/Fe t_{2g} band with down-spin (CT excitation) locates at ≈ 3.9 eV. These results are in good agreement with the density-functional calculation.⁵

ACKNOWLEDGMENTS

The authors would like to thank H. Sawada, K. Terakura, T. Kimura, and T. Manako for enlightening discussions. This work, partly supported by NEDO (New Energy and Industrial Technology Development Organization of Japan), was performed under the joint research agreement between National Institute for Advanced Interdisciplinary Research (NAIR) and Angstrom Technology Partnership (ATP).

¹F. S. Galasso, in *International Series of Monographs in Solid State Physics*, edited by R. Smoluchowski and N. Kurti (Pergamon, London, 1969).

²F. K. Patterson, C. W. Moeller, and R. Ward, *Inorg. Chem.* **2**, 196 (1963).

³F. S. Galasso, F. C. Douglas, and R. J. Kasper, *J. Chem. Phys.* **44**, 1672 (1966).

⁴M. Itoh, I. Ohta, and Y. Inaguma, *Mater. Sci. Eng., B* **41**, 55 (1996).

⁵K.-I. Kobayashi, T. Kimura, H. Sawada, K. Terakura, and Y. Tokura, *Nature (London)* **395**, 677 (1998).

⁶H. Sawada and K. Terakura (unpublished).

⁷W. E. Pickett, *Phys. Rev. B* **57**, 10 613 (1998).

⁸H. Y. Hwang, S.-W. Cheong, N. P. Ong, and B. Batlogg, *Phys. Rev. Lett.* **77**, 2041 (1996).

⁹A. Gupta, G. Q. Gong, G. Xiao, P. R. Duncombe, P. Lecoeur, P. Trouiloid, Y. Y. Wang, V. P. David, and J. Z. Sun, *Phys. Rev. B* **54**, R15 629 (1996).

¹⁰C. M. Hurd, *The Hall Effect in Metals and Alloys* (Plenum, New York, 1972).

¹¹J. A. Osborn, *Phys. Rev.* **67**, 351 (1945).

¹²K. Kadowaki and S. B. Woods, *Solid State Commun.* **55**, 507 (1986).

¹³J. V. Kranendonk and J. H. Van Vleck, *Rev. Mod. Phys.* **30**, 1 (1958).

¹⁴T. Arima, Y. Tokura, and J. B. Torrance, *Phys. Rev. B* **48**, 17 006 (1993).